

Impact of Power-to-Gas on distribution systems with large renewable energy penetration

Andrea Mazza, Fabio Salomone, Francesco Arrigo, Samir Bensaid, Ettore Bompard, Gianfranco Chicco

PII: S2590-1745(20)30025-8
DOI: <https://doi.org/10.1016/j.ecmx.2020.100053>
Reference: ECMX 100053

To appear in: *Energy Conversion and Management: X*

Received Date: 22 December 2019
Revised Date: 23 June 2020
Accepted Date: 14 July 2020

Please cite this article as: A. Mazza, F. Salomone, F. Arrigo, S. Bensaid, E. Bompard, G. Chicco, Impact of Power-to-Gas on distribution systems with large renewable energy penetration, *Energy Conversion and Management: X* (2020), doi: <https://doi.org/10.1016/j.ecmx.2020.100053>

This is a PDF file of an article that has undergone enhancements after acceptance, such as the addition of a cover page and metadata, and formatting for readability, but it is not yet the definitive version of record. This version will undergo additional copyediting, typesetting and review before it is published in its final form, but we are providing this version to give early visibility of the article. Please note that, during the production process, errors may be discovered which could affect the content, and all legal disclaimers that apply to the journal pertain.

Impact of Power-to-Gas on distribution systems with large renewable energy penetration

1 Andrea Mazza^{*,1}, Fabio Salomone², Francesco Arrigo¹, Samir Bensaid², Ettore Bompard¹, Gianfranco Chicco¹

2 *Corresponding author, E-mail address: andrea.mazza@polito.it (A. Mazza)

3 ¹Dipartimento Energia “Galileo Ferraris”, Politecnico di Torino, corso Duca degli Abruzzi 24, 10129 Torino, Italy

4 ² Dipartimento di Scienze Applicate e Tecnologia, Politecnico di Torino, corso Duca degli Abruzzi 24, 10129 Torino, Italy

7 Abstract

8 The exploitation of the Power-to-Gas (PtG) technology can properly support the distribution system operation in case of large
9 penetration of Renewable Energy Sources (RES). This paper addresses the impact of the PtG operation on the electrical distribution
10 systems. A novel model of the PtG plant has been created to be representative of the entire process chain, as well as to be
11 compatible with network calculations. The structure of the model with the corresponding parameters has been defined and validated
12 on the basis of measurements gathered on a real plant. The PtG impact on the distribution systems has then been simulated on two
13 network models representing a rural and a semi-urban environment, respectively. The testing has been carried out by defining a set
14 of cases that contain critical situations for the distribution network, caused by RES plant placement. The objectives of the
15 introduction of PtG are the reduction of the reverse power flow, as well as the reduction of the overcurrent and overvoltage issues in
16 the distribution system. The results obtained from annual simulations lead to considerable reduction (from 78 to 100%) of the
17 reverse power flow with respect to the base case, and to alleviating (or even solving) the overcurrent and overvoltage problems of
18 the networks. These results indicate PtG as a possible solution for guaranteeing a smooth transition towards decarbonized energy
19 systems. The capacity factors of the PtG plants largely vary depending on the network topology, the RES penetration, the number of
20 the PtG plants and their sizes. From the cases tested, the performance in a rural network (where the minimum capacity factor is
21 about 50%) resulted better than in a semi-urban network (where the capacity factor values range between 21% to 60%).

23 Keywords

24 Distribution System, Energy transition, Power-to-Gas, Renewable Energy Sources, Storage.

25 1. Introduction

26 In the last years, the increase of Renewable Energy Sources (RES) has changed the paradigm of the distribution system
27 operation, by imposing a shift from the traditional case of a completely passive network to a more and more active network hosting
28 an increasing share of local generation. The local generation is variable during time and can create different issues, such as i) reverse
29 power flow (occurring when the distribution system injects power into the transmission system), and ii) operational constraint
30 violations (in terms of voltage and current limits). For solving these problems without the RES production curtailment, the excess of
31 local generation should be converted and stored in appropriate forms.

32 The choice of the type of storage to be used depends on the need to use more power (generally with relatively short duration) or
33 more energy (from equipment that guarantee longer autonomy). Power-to-Gas (PtG) is a solution that can exploit the excess of
34 electricity from the local generation system to produce and store gas, then using the stored gas at a later time for different purposes.
35 These characteristics make PtG adapt to be integrated into multi-energy systems [1], [2] and to participate in the energy system
36 operation in a flexible way [3].

37 In general, PtG plants can be divided into two main product chains:

- 38 • *Power-to-Hydrogen*, where the excess of electricity from RES is transformed in hydrogen [4]
- 39 • *Power-to-Methane*, where the hydrogen produced is converted in methane through methanation [5]

40 This paper focuses on the second production chain and aims to study the integration of a PtG plant into a high-RES
41 distribution system.

42 In the literature, there are relatively few studies that combine both PtG and distribution systems. In [6], the authors have
43 investigated the use of an electrolyser as an alternative for network expansion in case of high photovoltaic (PV) penetration. A
44 real network has been modelled and the size of the electrolyser has been obtained by considering the same effect reached by
45 cable substitution. The techno-economic analysis has highlighted that the profitability is greatly depending on the local excess of
46 RES [7]. More in detail, RES electric excess has been used for sizing of the PtG plant capacity, reaching an overall PtG plant
47 efficiency of about 77% (on a LHV basis) and a utilization factor of about 30% [7]. These results have been obtained both
48 optimising the thermal integration between the methanation unit and the electrolyser, and analysing the management of each
49 equipment [7]. The use of a low-voltage (LV) electrolyser has been studied by predicting the temporal variation of excess energy
50 occurring in low voltage networks at 2030 and by identifying appropriate electrolyser capacities, while not considering any
51 network topologies, but only an equivalent energy balance at a single node [8]. In [9], the mitigation effect of electrolysers on the
52 reverse power flow has been exemplified on a LV grid. The evaluation of the use of power-to-methane chain in case of
53 distribution systems characterised by an excess of wind production has been analysed in [10]. The study has been based on the
54 consumption of gas and electricity of a local area, and the use of combined heat and power (CHP) plants locally installed has
55 been considered as well. In [11], the authors have focused on voltage regulation in active power distribution systems, by
56 presenting a new algorithm for the real time scheduling of PtG and Gas-to-Power (GtP) plants by considering also arbitrage
57 opportunities. In [12], the authors have presented a voltage control strategy by coordinating both the On-Load Tap Changer and
58 an alkaline electrolyser modelled dynamically as in [13]. The same electrolyser model has been used in [14] for studying how the
59 electrolyser can be optimally designed and installed for facing the increase of RES in future active distribution networks. The
60 alleviation of reverse power flow, line congestions and power losses in integrated power and gas network has been studied in
61 [15]–[17], respectively. In those cases, the authors have presented three different scheduling algorithms to properly deploy
62 power-to-methane and GtP conversion unit for distribution network support. The constraints of the chemical plants have been
63 represented in terms of minimum and maximum power and gas flow of the plants.

64 All the above papers have modelled the PtG units as “black boxes” without considering the physical connections existing
65 among the different plant parts, and thus also auxiliary services (such as compression systems) have been missed by the
66 modelling aspects. Thanks to the multi-disciplinary team composing the project STORE&GO [18], the complete model of a PtG
67 plant¹ has been created and then included in a power flow calculation. For representing the effect on different seasons, the annual
68 irradiation profiles have been considered with reference to the installation sites of the demonstration plants of the project.
69 Furthermore, for understanding the effect on different network topologies, two realistic network models have been introduced to

¹ From this point, with PtG plant only the power-to-methane chain will be indicated.

70 show the effect on both rural and semi-urban grids. Typical load profiles have been included to represent the variability of the
71 loads in time. Great attention has been devoted to the case study creation, by considering different possible positions of the PV
72 plants in the grid.

73 Regarding the electrical point of view, the PtG plant is a particular type of load, and as such it has to be properly modelled in
74 a power flow calculation tool. PtG plant modelling is an open research issue, especially because of the need of providing a sound
75 validation of the model on the basis of real case applications. On the basis of the previous considerations, this paper presents a
76 number of specific contributions to the modelling and exploitation of PtG in distribution systems, namely:

- 77 1. The PtG plant modelling is addressed in order to formulate a steady-state model of PtG to be incorporated in the power flow
78 equation solvers. The validation of the model is carried out on the basis of measurements collected from a real PtG plant.
- 79 2. The impact of PtG on the distribution system operation is then studied through simulations in steady-state conditions.
80 Different loading and RES penetration are considered for reproducing different network issues that may be alleviated by
81 using PtG plants. Dedicated cases are created with different RES penetration, by locating the RES sources at network nodes
82 that correspond to critical conditions for the amount of reverse power flows, as well as for the presence of overcurrent and
83 overvoltage issues in the distribution network.

84 The rest of the paper is organised as follows. Section 2 presents the characteristics of the PtG plant modelled and highlights
85 the modularity of the proposed model. Section 3 focuses on the creation of the case studies, by considering different PV
86 penetration and location in the two networks. Section 4 shows the results, whereas Section 5 provides the concluding remarks.

87 **2. PtG plant model**

88 The PtG plant consists of a low temperature-based electrolyser (LTE), a buffer and a methanation unit. A simplified scheme
89 of the PtG process is illustrated in Figure 1. The LTE converts liquid water into gaseous oxygen at the anode and gaseous
90 hydrogen at the cathode through electrolysis [7], [19]–[22]. According to the literature, the efficiency of the electrolysis ranges
91 between 55% to 70% (on a LHV basis) [7], [23], [24]. The hydrogen produced within the LTE could be stored in a tank or sent
92 to the methanation unit. The hydrogen is mixed in stoichiometric ratio with carbon dioxide (H_2/CO_2 molar ratio equal to 4) in
93 order to supply the methanation unit that produces synthetic natural gas (SNG) [7], [19], [22].

94

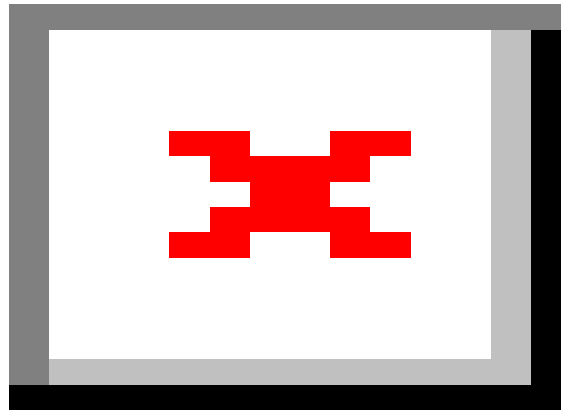


Figure 1. Simplified low temperature-based Power-to-Gas process scheme considering H_2 storage.

In addition, the main characteristics of the PtG are summarized in Table 1.

Table 1. Characteristics of the PtG plant.

Parameter	Value	Parameter	Value
LTE operating temperature	80 °C	CO ₂ conversion within the methanation unit	98.5 %
LTE and methanation unit pressure	15 bar	Inlet – outlet temperature of the cooling water	28 – 32 °C
H ₂ tank maximum pressure	60 bar	Coolant temperature in the methanation unit	250 °C
Compression efficiency	75 %	Power-to-hydrogen efficiency (LHV basis)	57.6 %

2.1 Characteristics of the electrolyser

A low temperature-based electrolyser is characterised by a power-to-hydrogen efficiency, whereas the methanation unit is characterised by a certain value of the CO₂ conversion efficiency (i.e., 98.5% [7], [19], [25]).

The PtG model has been built considering the dynamics (start-ups, shutdowns and partial loads) of a real plant installed in the demonstration site of Falkenhagen (Germany), whose process is based on Alkaline Electrolysis (AEC). This plant consists of a 2 MW AEC-electrolyser, which was composed of 6 AEC modules (330 kW each one). The electrolysis technology considered has minimum load $P_{MIN}=20\%$ [23] and power-to-hydrogen efficiency $\eta_{H_2} = 57.6\%^2$ (real data).

The characteristics of minimum load and efficiency of the AEC technology has been directly provided by the Falkenhagen

² The efficiency refers to the Lower Heating Value.

109 plant managers, based on their long-time experience in the plant operation. It is worth noting that the AEC efficiency is in line
 110 with the related literature [24], [26]. Regarding the minimum load of the electrolyser (i.e., the power to be provided for
 111 producing the minimum amount of H₂), the values existing in the literature are even lower than 20 % but they may lead to
 112 problems (see for example [23], [27]). The modularity of these technologies simplifies the management of the electrolyser,
 113 moreover each module could be maintained in hot stand-by if there is not enough electrical energy for supplying the PtG plant.

114 On the one hand, the electrolyser has a wide rangeability thanks to its modularity. On the contrary, the methanation reactors
 115 have a narrow rangeability due to the kinetics of the methanation reaction [25], [28]. More specifically, according to the
 116 literature [25], the reactors are conceived as tube-bundles refrigerated by evaporating water at 250 °C. The methanation reaction
 117 is extremely exothermic [28], [29]; hence, the tube diameter must be small for avoiding too high radial thermal profiles.
 118 Obviously, the design of a methanation reactor is made for the nominal productivity; however, the residence time increases (and
 119 the gas hourly space velocity decreases) reducing the productivity. Consequently, the heat generation profile along the axis of the
 120 reactor becomes narrower and more intense; in addition, the overall heat exchange coefficient decreases [19], [25]. Therefore, it
 121 could cause problems of thermal management, hot spots and local deactivation of the Ni/γ-Al₂O₃ catalyst (i.e. sintering) [7],
 122 [28]–[30]. Hence, each reactor could be parallelized in 3 or 4 bundles in order to increase the rangeability of the PtG plant, for
 123 instance, from about 60-110% (i.e., only one bundle for each reactor) to about 20-110% (i.e., three bundles in parallel for each
 124 reactor). For all these reasons, the best option is to maintain the methanation unit at least at the minimum operative load.

125 The model developed in this work, as additional feature, considers also all the auxiliary consumptions, which can be easily
 126 adjusted according to the actual PtG plant layout. More in detail, the energy consumption of a compressor (E_{compr} , W) was
 127 calculated according to equation (1) [31], where Z is the compressibility factor that was assumed unitary, R (8.314 J mol⁻¹ K⁻¹) is
 128 the ideal gas constant, T_{in} (K) is the inlet temperature, \dot{n}_{in} (mol s⁻¹) is the inlet molar flow rate, γ is the heat capacity ratio, and
 129 η_{compr} is the compression efficiency, which was set equal to 70% and p_{in} and p_{out} represent the inlet and outlet pressure,
 130 respectively. In addition, multistage compression was considered if the compression ratio ($p_{\text{out}}/p_{\text{in}}$) was greater than 4.

$$E_{\text{compr}} = Z \cdot R \cdot T_{\text{in}} \cdot \frac{\gamma \cdot \eta_{\text{compr}}}{\gamma - 1} \cdot \left[\left(\frac{p_{\text{out}}}{p_{\text{in}}} \right)^{\frac{\gamma - 1}{\gamma \cdot \eta_{\text{compr}}}} - 1 \right] \cdot \dot{n}_{\text{in}} \quad (1)$$

131 Moreover, the methanation unit and the electrolyser require an additional electric consumption due to heat dissipations caused
 132 by natural convection [7], if they are maintained in hot stand-by.

133 2.2 The electrolyser model

134 The dynamic behaviour of the AEC-electrolyser has been obtained from the analysis of a test carried out at the Falkenhagen
 135 plant (shown in Figure 2).

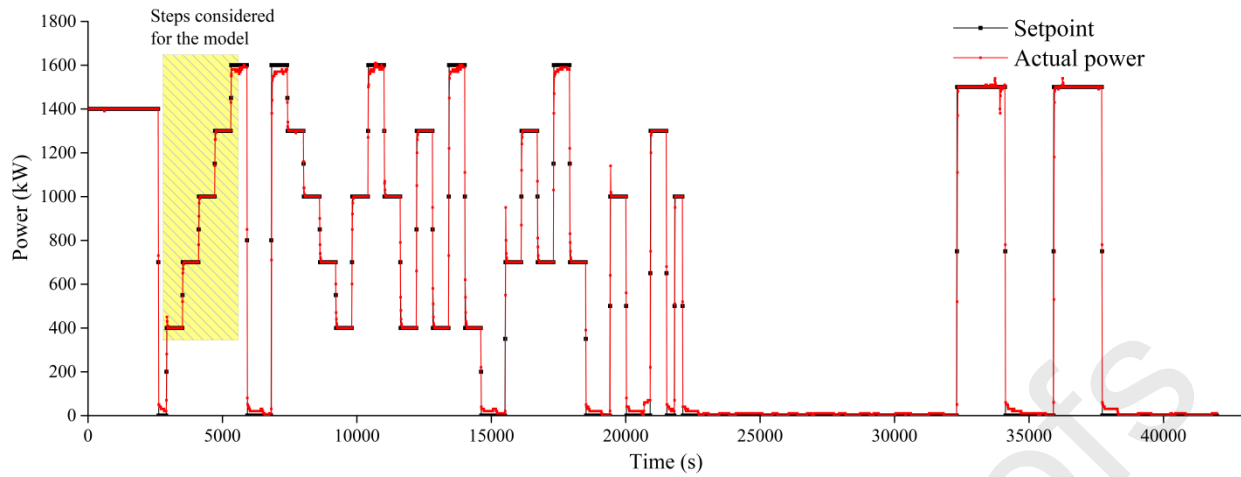


Figure 2. Falkenhagen test on an AEC-based electrolyser

The test had duration of about 11.5 h and highlighted that the AEC-based electrolyser had a fast response when the setpoint changed. Therefore, its response could be modelled for the purpose of forecasting the behaviour of the AEC-based electrolyser when it is coupled with an intermittent RES-based electrical profile. It is worth mentioning that during the test, the set point of the electrolyser was periodically changed with steps of different amplitude to explore a large number of operating conditions.

The easiest model to describe the AEC-based electrolyser behaviour is a first order system with delay, which is characterised by three parameters; the mathematical model of its response to a step is described by means of equation (2) [32]–[34]:

$$\begin{cases} y(t) = 0 & \text{If } t < \alpha \\ y(t) = A \cdot K \cdot \left[1 - \exp\left(-\frac{t-\alpha}{\tau}\right) \right] & \text{If } t \geq \alpha \end{cases} \quad (2)$$

In this equation, $y(t)$ is the actual power of the AEC-based electrolyser (MW) at the time step t (s), A is the step amplitude of the set point (MW), K is the gain of the system, α is the time delay of the response (s), τ is the time constant of the system (s). The gain K can be evaluated by means of equation (3), where $y(\infty)$ is the actual power of the electrolyser after a large period of time (stationary condition):

$$K = \frac{y(\infty)}{A} \quad (3)$$

The two time parameters (α and τ) have been estimated by means of the Sundaresan and Krishnaswamy's method [35], according to equations (4) and (5), respectively. The two parameters were calculated using two characteristic points of the response curve: t_1 represents the time in which the response reaches 35.3% of the stationary value $y(\infty)$, while t_2 is estimated as the time in which the response reaches 85.3% of the final value $y(\infty)$:

$$\alpha = 1.3 \cdot t_1 - 0.29 \cdot t_2 \quad (4)$$

$$\tau = 0.67 \cdot (t_2 - t_1) \quad (5)$$

For the purpose of evaluating these three parameters, four steps with the same amplitude (i.e., 0.3 MW) have been considered, by obtaining the parameters shown in Table 2. These steps are highlighted in Figure 2 between 40 min and 100 min of the test.

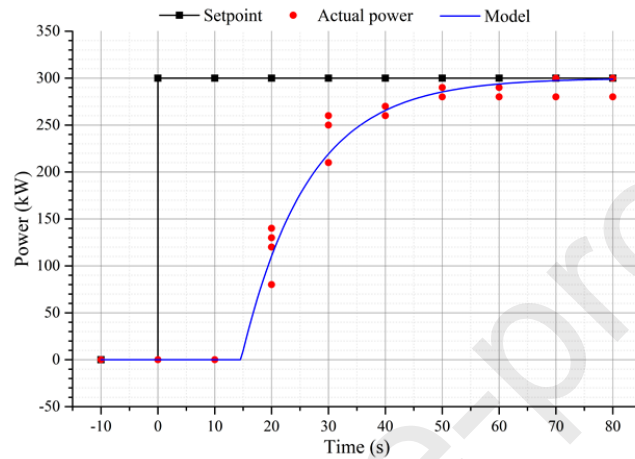
155

Table 2. Characteristics of the low temperature-based electrolyser.

Parameter	Value
K	1
α [s]	14.62
τ [s]	11.73

156

157 The fit between the model output and the real data is shown in Figure 3.



158

159 Figure 3. AEC-based electrolyser response model estimated using Falkenhagen test data (first order system with delay). It is worth noting that
 160 the experimental data (red spots) refer to the four steps considered for the modeling, as mentioned in the text. For comparing the behavior of
 161 the response, the starting values of the real steps were shifted to zero (baseline), and thus some data are overlapping.

162

2.3 Simulation algorithm of the PtG plant model

163

The flowchart of the simulation algorithm (called in the sequel *function_PtG*) is shown in Figure 4.

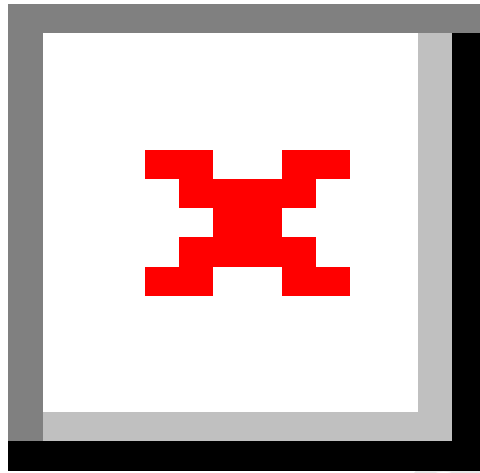


Figure 4. Flowchart of the algorithm (function_PtG)

164
165

166 The simulation algorithm consists of the following main instructions:

- 167 • *Setpoint*: the setpoint is defined as the theoretical maximum operative power at which the electrolyser may work. This
168 maximum can correspond to either the power provided by the grid (when it is lower than the nominal power of the
169 electrolyser) or the nominal power of the electrolyser (in the case it exceeds the nominal power of the electrolyser).
- 170 • *Actual power*: it represents the actual electric consumption that could be calculated using the dynamic model of the AEC-
171 based electrolyser (Section 2.2).
- 172 • *Hydrogen production*: the hydrogen flow could be evaluated taking into account the efficiency of the electrolyser.
- 173 • *Hydrogen tank management*: if the electrolyser is operative, a minimum hydrogen flow feeds the methanation unit.
174 Beyond this, certain amount of hydrogen is sent to a hydrogen tank until the tank is completely full (the priority is filling
175 the tank). This operation allows to decouple the methanation unit from the electrolyser. When the electrolyser is not
176 operative, the stored hydrogen is fed to the methanation unit, for producing continuously SNG. In this case, the
177 methanation unit works at the minimum power load; when the hydrogen tank is completely empty, it could be turned off
178 and remain in hot standby conditions³. More in detail, H₂ produced in the LTE could be split into two streams. During the
179 filling of the H₂ tank three configurations have to be considered:

³ A hot standby condition (it means that the equipment is maintained at the operative temperature conditions with auxiliary energy, in order to ensure a fast start up) was assumed for the main equipment (electrolyser and methanation unit).

- If the H₂ tank is empty, its pressure is lower than the operative pressure of both the LTE and the methanation unit. Therefore, the compressor (P-102) is useless and the H₂ tank could be partially filled using stream 9 until the storage pressure is equal to the operative pressure of the LTE.
- If the H₂ tank is partially filled, its pressure ranges between the operative pressure of the LTE and the maximum storage pressure. Therefore, the compressor (P-102) is used for filling the tank until it is completely full.
- If the H₂ tank is completely full, the produced H₂ is directly fed to the methanation unit using stream 16.

If the LTE does not produce H₂, the methanation unit could be fed using the stored H₂. In this case, three configurations could be possible:

- If the tank pressure is higher than the operative pressure of the methanation unit, H₂ could be fed to the methanation unit through stream 14.
- If the tank is emptying, H₂ could be fed to the methanation unit using the compressor P-103 until the tank is completely empty.
- If the H₂ tank is empty and no electricity is available for producing H₂, the methanation unit must be turned off (shutdown of the PtG plant).

- *Auxiliary consumptions*: all the consumptions of the auxiliary items of equipment are related to the amount of produced hydrogen. Firstly, the hydrogen could be compressed; secondly, the carbon dioxide has to be compressed; thirdly, the water has to be pumped and lastly it must be heated up to the temperature of the electrolyser.
- *Control of the setpoint*: the setpoint power of the electrolyser must be recalculated considering the new auxiliary consumptions, because the available electricity is comparable with the power absorbed by the electrolyser. This affects the power withdrawn from the power grid.
- *Methanation unit*: the amount of SNG could be calculated using the CO₂ conversion, or alternatively, the hydrogen-to-SNG efficiency.

3. Creation of the case studies

As widely shown in literature (for example in [36]), the installation of large share of RES can create the following issues in the electrical networks:

- *Reverse power flow (RPF)*: on the one hand, a reverse power flow affects the transmission system because the point of connection between transmission and distribution system becomes equivalent to a non-controllable active node. On the other hand, the presence of reverse power flow can create issues also at the distribution system, for example in terms of not proper protection schemes. Usually, these problems are nowadays solved by cutting the excess of production or using some pilot battery-based storage [37].
- *Overcurrent (OC)*: the large share of RES can create overcurrents along the feeders. These overcurrents can affect only a portion of the network (e.g., the last portion) or the entire network, depending on the level of load and distributed generation, together with the geographical position of the PV plants.
- *Overvoltages (OV)*: this problem is characteristic especially of rural networks, composed of long feeders (also up to 10 km), and characterized by a high R/X ratio, which leads to have to voltage levels changes strictly linked with the active power flowing in the grid branches.

It is worth noting that the presence of reverse power flow leads the network to operate in an alert condition, whereas the presence of overcurrent and overvoltage are symptoms of an emergency condition (because directly affecting the operational

218 constraints of the network) [38] and the distribution system operators needs to solve these problems as soon as possible, by
219 making use of different approaches which can even result in lower quality of service (e.g., load disconnections). So, the
220 simulations carried out starting from conditions in which the network constraints are not satisfied (even though these conditions
221 do not correspond to real situations) have the goal to show, in very extreme cases, how the potential use of PtG can alleviate also
222 these problems.

223 The creation of the case studies needs the proper placement of the PV plants. In this study, the placement of the PV plants has
224 been carried out by using two different approaches:

- 225 • *Topological approach*: the PV plants have been installed according to the length of the network lines.
- 226 • *Losses Allocation Factors-based approach*: in this case, the approach shown in [39] and based on [40] has been adopted.
227 A detailed analysis on the implication of the use of the loss allocation for distribution system analysis can be found in
228 [41].

229 These approaches are followed by using a series of assumptions on the model of the distribution system, namely, (i) the power
230 flow is calculated as an equivalent single-phase circuit. This is justified in medium voltage networks (to which PtG is connected,
231 because of its size), where loads and generations are usually distributed in a relatively uniform way on the three phases; (ii) the
232 distribution system is analysed in time as a succession of steady state conditions, in which constant average power
233 withdrawn/injected by loads and local generations in every time step are considered for the power flow calculations. This also
234 implies that the frequency is considered constant (at 50 Hz) during the entire simulation horizon. The use of more detailed
235 dynamic models for the electrical system, which would be able to represent real-time phenomena at milliseconds to seconds
236 scale, is not needed for the type of analysis carried out in this paper; and (iii) the network parameters are known and constant
237 during the entire simulation horizon, which is a usual assumption made in the power flow calculations. This implies that external
238 conditions (such as temperature, etc.) do not affect the parameters (e.g., loads or branch resistances).

239

240 3.1 The network samples

241 This work considers two network samples:

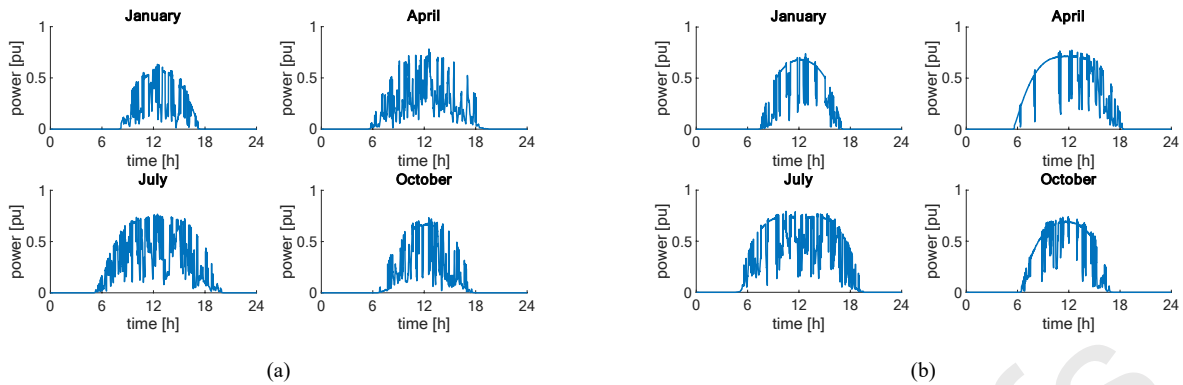
- 242 • *Semi-urban network*, adapted from the one shown in [42], by adding time-varying loads with different profiles. For this
243 network only the topological PV placement has been applied [43].
- 244 • *Rural network*, developed in the project *Atlantide* [44]. For this network, both PV placement methods have been used.

245 The two network samples aim to represent different network topologies and allow to emulate the distribution systems in the
246 areas where the demo sites of the project are installed. The two demo sites are in installed in Solothurn (Switzerland) and in
247 Troia (Italy). In particular, the network semi-urban refers to Solothurn area, whereas the rural network refers to Troia area.

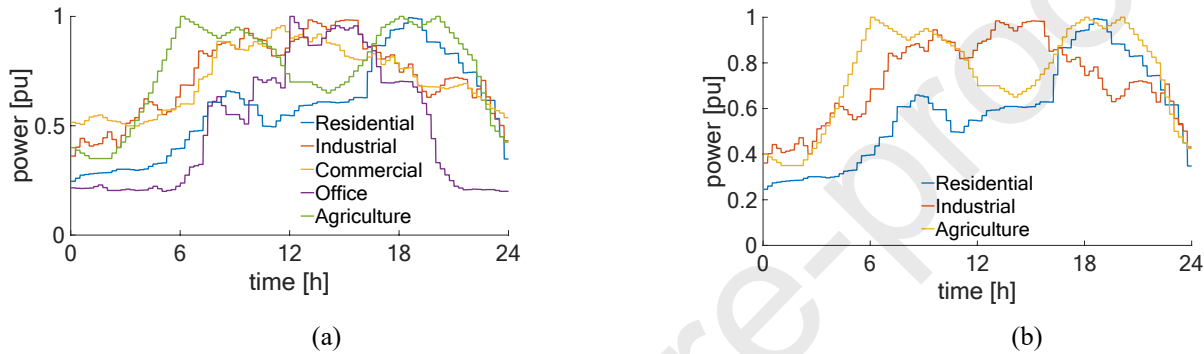
248 Few samples referring to daily PV profiles in different months used for the two networks are shown in Figure 5, whereas the
249 load profiles used are shown in Figure 6. It is worth noting that the PV profiles are different for the two network samples because
250 referring to two different geographic locations, and have been obtained from [45].

251 Moreover, during the night time the PtG plant is supplied by the main grid to guarantee the continuous operation of the plant
252 in compliance with its minimum power specified in Section 2.1 (i.e., $P_{\text{MIN}}=20\%$).

253



254 *Figure 5. PV profiles considered for building the case studies. Four months have been considered (January, April, July and October): (a) semi-*
 255 *urban network and (b) rural network*



256 *Figure 6. Load profiles used in (a) semi-urban network and (b) rural network [44].*

257 3.2 Introduction of the PtG plant model into the calculation loop of the network operation

258 The model of the PtG explained in Section 2 needs to be integrated in the network solver, which is based on the Backward
 259 Forward Sweep (BFS) method [46]. The response of the PtG unit is modelled as a first order system and solved through the
 260 Matlab[®]-embedded solver ode45. The calculation loop is shown in Figure 7. The variables used in the calculation loop are
 261 presented in Table 3.

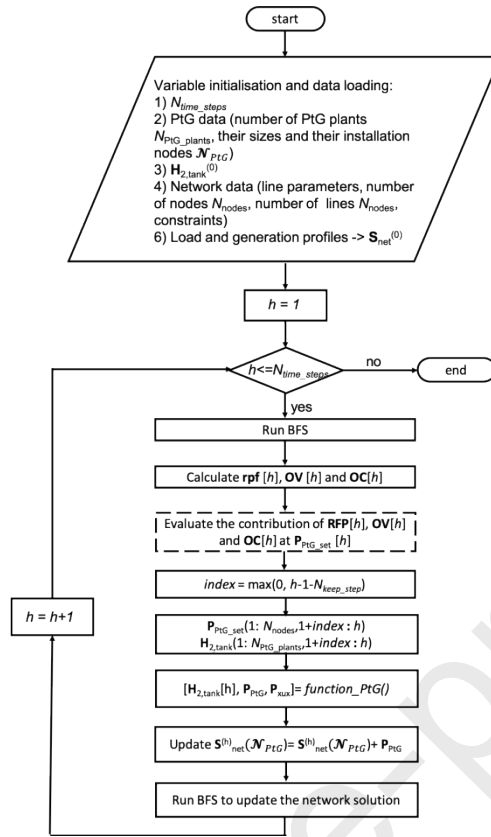


Figure 7. The main calculation loop of the distribution system. The function called function_PtG represents the PtG complete model.

Table 3. Input parameters of the main calculation loop

Inputs	Description
N_{time_steps}	Number of time steps of the analysis
PtG data	Number of the PtG plants N_{PtG_plants} , their positions (indicated by the nodes contained in the set \mathcal{N}_{PtG}) and their sizes
$\mathbf{H}_{2,tank}^{(0)}$	Initial value of the matrix of dimensions $\{N_{PtG_plants}, N_{time_steps}\}$ representing the volume of H_2 in the tank in time
N_{keep_steps}	Number of points for running PtG model
Network data	Number of nodes N_{nodes} , number of branches $N_{branches}$, line parameters, incidence matrix, rate nodal power, lines thermal limits
Load and generation profiles	Load and generation profiles for evaluating the initial value of the matrix $\mathbf{S}_{net}^{(0)}$, i.e., the net nodal power (dimensions $\{N_{nodes}, N_{time_steps}\}$)
RPF	Matrix of dimensions $\{N_{branches}, N_{time_steps}\}$ containing the value of reverse power flow at every time step
OC	Matrix of dimensions $\{N_{branches}, N_{time_steps}\}$ containing the value of overcurrent for every branch during the time span of simulation
OV	Matrix of dimensions $\{N_{branches}, N_{time_steps}\}$ containing the value of overvoltages for every node during the time span of simulation
\mathbf{P}_{PtG_set}	Matrix of dimensions $\{N_{PtG_plants}, N_{time_steps}\}$ containing the set points of the PtG plants
\mathbf{P}_{PtG}	Matrix of dimensions $\{N_{PtG_plants}, N_{time_steps}\}$ containing the actual power that the PtG plants are able to accept (linked to their sizes)

265 After having loaded the inputs, the algorithm runs the BFS for the first time: this is requested for defining the network

266 conditions (i.e., nodal voltages and branch currents). On the basis of this, the h -th column of the matrix **RPF** (containing the
 267 value of RPF at every branch the interaction h) is updated. At the same time, the h -th columns of both matrices **OV** and **OC** are
 268 updated with the values of overvoltage and overcurrent, respectively. On the basis of the above values, a *compound set point*
 269 $\mathbf{P}_{PtG_set}[h]$ is produced, and is referred to the RPF and overcurrent value of the branch upstream with respect to the node of the PtG
 270 plant, while the contribution regarding the overvoltage is linked to the overvoltage value of the node where the PtG plant has
 271 been installed as presented in equation (6), i.e.,

$$\mathbf{P}_{PtG_set}[h] = f(\mathbf{RPF}[h], \mathbf{OV}[h], \mathbf{OC}[h]) \quad (6)$$

272 In particular, the different set point components are set as follows:

- 273 • *Component referring to the RPF*: this component is equal to value of power needed for eliminating the reverse power
 274 flow in the upstream branch with respect to the node where the PtG plant is installed.
- 275 • *Component referring to the OC*: this component is equal to the value of power that, absorbed from the PtG plant, would
 276 help to reduce (at 80% of the thermal limit) the current flowing in the upstream branch with respect to the node where the
 277 PtG plant is installed.
- 278 • *Component referring to the OV*: this component is equal to the value of power that, absorbed from the PtG plant, would
 279 help to reduce (at 1.05 pu) the voltage of the node where the PtG plant is installed.

280 3.3 Installation and sizing of the PtG plants

281 The study of the impact of the PtG plants on the distribution system requires to i) choose the node where the plants are
 282 installed and ii) their sizes. These two elements are requested by the calculation loop shown in Figure 7, and in this work have
 283 been solved by applying the Simulated Annealing (SA) method [47]. It is worth noting that the main goal of this paper is not
 284 introducing a new algorithm for the siting and sizing of the PtG plants; but creating meaningful case studies to get insights
 285 regarding the *impact of the PtG plants* on distribution system operation. However, the step regarding the siting and sizing is
 286 requested as preliminary task, for emulating the process that, in the future, could bring to rationally install a defined number of
 287 MW-scale PtG plants. Few notes regarding the use of the SA in this work are reported in Appendix.

288 The objective functions used in the algorithm have as main variables the value of reverse power flow, overcurrent and
 289 overvoltage of the network. In particular, the network with the installed PtG plants (denoted as **X**) can be affected by:

- 290 • Only reverse power flow
- 291 • Reverse power flow and overcurrent
- 292 • Reverse power flow and overvoltage
- 293 • The combination of the last two cases

294 All the cases make use of a penalised objective function where the constraints of the problem are integrated within the
 295 objective function through penalisation factors indicated with the Greek letter ρ . This approach allows driving the optimisation
 296 towards solution with no constraint violations. In particular, the operational constraints are the voltages V_j of the network nodes
 297 and the currents I_b flowing in the network branches, which have to remain inside the following ranges:

- 298 • $V_j^{(min)} \leq V_j \leq V_j^{(max)}$, with $j \in \mathbf{J}$, where \mathbf{J} denotes the set of nodes. The node voltage is usually expressed in per unit (pu) with
 299 respect to the nominal voltage (i.e., $V_j=1$ means that the voltage value of the node j is equal to the nominal voltage of the
 300 system). Usual values of the extremes of the range are $V_j^{(min)} = 0.9$ pu and $V_j^{(max)} = 1.1$ pu.
- 301 • $I_b \leq I_b^{(th,max)}$, with $b \in \mathbf{B}$, where \mathbf{B} denotes the set of branches. The value of $I_b^{(th,max)}$ is strictly depending on the

conductors installed.

The objective function at the iteration k of the method in case of existence of the sole reverse power flow is shown in equation (7):

$$f_k(\mathbf{X}) = \frac{RPF_k}{RPF_0} \cdot \left(1 + \sum_{j \in \mathbf{J}} \rho_V \left(\frac{V_j^{(max)} - V_j^{(worst)}}{V_j^{(max)}} \right)^2 + \sum_{j \in \mathbf{J}} \rho_V \left(\frac{V_j^{(min)} - V_j^{(worst)}}{V_j^{(min)}} \right)^2 + \sum_{b \in \mathbf{B}} \rho_I \left(\frac{I_b^{(th,max)} - I_b^{(worst)}}{I_b^{(max)}} \right)^2 \right) \quad (7)$$

The penalised objective function at the iteration k is expressed in pu with respect to the value of the reverse power flow in the initial configuration. The reverse power flow is evaluated here through the number of minutes in which it is present during the entire period of analysis. The formulation penalises (through the factors ρ_V and ρ_I) all the configurations that do not respect the operational constraints (i.e., maximum and minimum voltage, and thermal limits) of the network. Thus, the constraints of the objective function (7) are the operational constraints of the network $V_j^{(max)}$, $V_j^{(min)}$ and $I_b^{(th,max)}$, for node j and branch b , respectively. For every node/branch the *worst* condition (e.g., the maximum current $I_b^{(worst)}$ during the day) is chosen as representative value to force the worst condition respects the imposed constraint.

When both overcurrent and reverse power flow exist in the initial configuration, the objective function is modified as reported in equation (8):

$$f_k(\mathbf{X}) = \left(\frac{RPF_k}{RPF_0} + \frac{OC_k}{OC_0} \right) \cdot \left(1 + \sum_{j \in \mathbf{J}} \rho_V \left(\frac{V_j^{(max)} - V_j^{(worst)}}{V_j^{(max)}} \right)^2 + \sum_{j \in \mathbf{J}} \rho_V \left(\frac{V_j^{(min)} - V_j^{(worst)}}{V_j^{(min)}} \right)^2 \right) \quad (8)$$

In this case, the objective function is still expressed in pu with respect to the initial configuration. The normalised sum of the minute of overcurrent and the minute of reverse power flow during the entire day are modified according to the product of the penalty factors and the value of the constraint violation. In this case, the constraints are the maximum and the minimum voltage values, indicated as $V_j^{(max)}$ and $V_j^{(min)}$, respectively.

The objective function in case both overvoltage and reverse power flow exist is shown in equation (9) and differs with respect to equation (8) only for the constraints considered, i.e., related to the branch thermal limits $I_b^{(th,max)}$ and the minimum nodal voltages $V_j^{(min)}$:

$$f_k(\mathbf{X}) = \left(\frac{RPF_k}{RPF_0} + \frac{OV_k}{OV_0} \right) \cdot \left(1 + \sum_{j \in \mathbf{J}} \rho_V \left(\frac{V_j^{(min)} - V_j^{(worst)}}{V_j^{(min)}} \right)^2 + \sum_{b \in \mathbf{B}} \rho_I \left(\frac{I_b^{(th,max)} - I_b^{(worst)}}{I_b^{(max)}} \right)^2 \right) \quad (9)$$

When all the issues listed above (i.e., reverse power flow, overvoltages and overcurrents) affect the grid, then the objective function is changed to solve them, as shown in equation (10):

$$f_k(\mathbf{X}) = \left(\frac{RPF_k}{RPF_0} + \frac{OV_k}{OV_0} + \frac{OC_k}{OC_0} \right) \cdot \left(1 + \sum_{j \in \mathbf{J}} \rho_V \left(\frac{V_j^{(min)} - V_j^{(worst)}}{V_j^{(min)}} \right)^2 \right) \quad (10)$$

It is worth noting that in eq. (9) the constraint related to the minimum voltage value is still considered as part of the penalized objective function, to avoid that the worst value reached by the voltages in the period under analysis $V_j^{(worst)}$ falls below the minimum allowed value $V_j^{(min)}$.

As the final comment, the above objective functions are chosen *a priori* according to the network issues that affect the distribution system under analysis.

4. Results and discussion

4.1 Annual simulation

4.1.1 Network performance indexes

Different PV penetrations have been assumed for the creation of the case studies. The penetration has been calculated in terms of *percentage the energy* provided by the PV plants with respect to the system passive load considering the PV production in July. In the case with 40% of PV penetration, the production in July covers 40% of the passive load. According to this, the PV penetration in other months varies following the different PV profiles.

The considered case studies and the existing problems in the different cases are shown in Table 4 and Table 5 for the semi-urban network and the rural network, respectively. The tables show entries different from zeros when that kind of problem exists, and the entry indicates the magnitude of the problem. The label “Pre” in the table indicates the magnitude of the problem without PtG installed, whereas the label “Post” refers to the condition when PtG plants have been installed. The RPF has been indicated in MWh, whereas the OC and OV are expressed in minutes.

The values refer to annual simulations. The two tables show the number of plants installed and, only for the rural network, the size of the plants as well. Due to the large number of plants installed in the case of semi-urban network, the sizes of the plants are summarised in Figure 8.

Table 4. Case studies for the semi-urban network

Case number	Length [km]*	PV penetration	RPF [MWh]		OC [min]		OV [min]		Number of PtG plants
			Pre	Post	Pre	Post	Pre	post	
1	$0 < L \leq 0.45$	40 %	11,298	9.37	-	-	-	-	7
2		80 %	151,920	33,654	90,616	35	-	-	20
3	$0.5 \leq L \leq 3$	40 %	10,213	31.4	430,087	6,978	3,356	0	12
4		60 %	71,272	7,165	2,388,634	25,156	900,407	0	17

*The length refers to the branches of the MV semi-urban network.

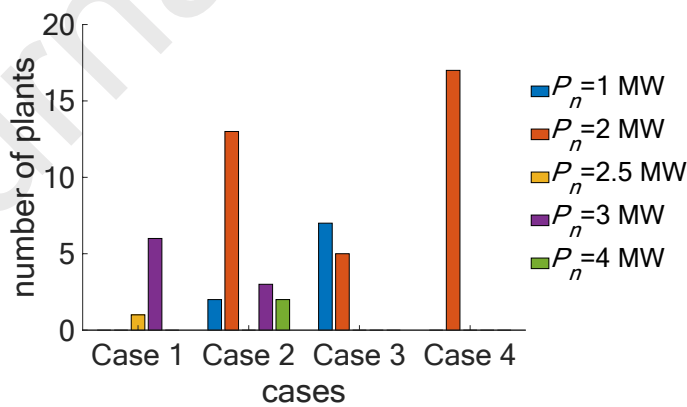


Figure 8. Number and sizes of the PtG plants installed in the semi-urban network

Table 5. Case studies for the rural network

Case	Method PV placement	Length* [km]	PV penetration	RPF [MWh]		OC [min]		OV [min]		Number of PtG plants	Size [MW]
				pre	post	pre	post	pre	post		

5	Topological	$0 < L \leq 0.9$	40%	266.27	0	-	-	-	-	1	2.5
6			80%	19,861	1633.9	165,047	0	504	-	4	2 (all)
7		$2 \leq L \leq 3$	40%	248.99	0.10	-	-	-	-	1	2
8			80%	19,206	3,337.4	-	-	276,329	0	4	2 (three plants) 1.5 (one plant)
9	Loss allocation	-	40%	167.90	0	-	-	-	-	2	2 (all)
10			80%	20,991	1868.4	-	-	-	-	4	2 (all)

350 *The length refers to the branches of the MV network

351

352 First of all, it is evident that, while in the rural network is possible to obtain cases with problems of overvoltages and reverse
353 power flow, in the semi-urban network is difficult to decouple overvoltage and overcurrent. This is linked with the nature of the
354 lines composing the networks, which are highly resistive for the rural network because mostly composed of long overhead lines.

355 It is worth noting that, as demonstrated through the rural network, the reverse power flow issue is not strictly linked to
356 overvoltage problems, but these two aspects can be decoupled through a suitable installation of PV generation (as the one
357 guaranteed by the procedure shown in [39]).

358 From the two tables it is evident that the deployment of PtG has a positive impact on alleviating the grid issues.

359 For the *semi-urban network*, in the cases in which the PV is installed at the end of lines with length L lying in the range $0 < L$
360 ≤ 0.45 , the impact of PtG is indeed powerful, because both cases reveal how the reverse power flow can be strongly reduced: in
361 fact, in case of PV penetration equal to 40% the reduction is over 99.9% (passing from almost 11.3 GWh to 9.37 MWh), whereas
362 with PV penetration equal to 80% the reduction is almost 78% (passing from almost 152 GWh to 34 GWh). In the cases with PV
363 plants installed at the end of lines with length L lying in the range $0.5 \leq L \leq 3$, the reduction of reverse power flow is stronger for
364 lower PV penetration (more than 99.6% with PV penetration equal to 40%), but is anyway high also with PV penetration equal
365 to 60% (the reverse power flow reduction reached almost 90%). Residual problems of overcurrents appear in all the cases except
366 Case 1.

367

368 By analysing the worst case (i.e., the one with PV penetration equal to 60%), these issues affect in total thirteen branches, and
369 the number of minutes in which the lines are overloaded lies between 4 to 5456 minutes, whereas the maximum overload
370 conditions at which they operate lies in the range between 2.24% and 13.39%, as shown in Table 6. The system operator has to
371 act for establishing again the proper network conditions, because the alleviation effect of the PtG deployment cannot solve
372 completely the overcurrent issues.

373 Table 6. Analysis of the overloaded lines in of semi-urban network, with 60% of PV penetration

Lines overloaded	Cumulative overload period [min]	Maximum overloading [%]
6	284	11.47
32	13	9.02
152	79	13.39
155	5032	9.05
156	4747	8.86
157	5456	10.10
159	2717	6.12

161	910	17.33
165	1395	2.43
169	4382	7.62
170	123	13.10
185	4	2.24
196	14	4.78

For the rural network, in the cases in which the PV is installed at the end of lines with length L lying in the range $0 < L \leq 0.45$, the impact of PtG is again powerful, because in one case (i.e., PV penetration equal to 40%) the reverse power flow is completely solved, whereas in the case with 80% of PV penetration the reverse power flow is strongly reduced, passing from 19.861 GWh to 1633.9 MWh (reduction of almost 92%). In the cases with PV plants installed at the end of lines with length L lying in the range $2 \leq L \leq 3$, the reduction of reverse power flow is stronger in case of lower PV penetration (almost 100% with PV penetration equal to 40%), but is anyway high also with PV penetration equal to 80% (the reverse power flow reduction reached almost 83%).

Finally, the case created with the rural network by using the loss allocation shows that the reverse power flow problem can be solved in case of 40% of PV penetration, whereas a residual reverse power flow remains for the case 80% (but even in this case the reduction is more than 90%).

4.1.2 Capacity factors

The successful use of PtG plants needs a justification in terms of plant use, i.e., a *capacity factor* high enough.

The capacity factor $C_f^{(i)}$ that refers to the i -th PtG unit is the ratio between the energy $E_{PtG}^{(i)}$ consumed by the i -th PtG unit during the simulation period Δt and the theoretical energy that the plant would be able to absorb during the same time period if it had consumed its nominal power; it was calculated according to equation (11):

$$C_f^{(i)} = \frac{E_{PtG}^{(i)}}{P_{n,PtG}^{(i)} \cdot \Delta t} \quad (11)$$

where $E_{PtG}^{(i)}$ is the energy consumed during the simulated time horizon Δt by the i -th PtG plant, and $P_{n,PtG}^{(i)}$ is the nominal power of the i -th PtG plant.

Figure 9 shows the capacity factors for the semi-urban network. It shows that in Case 1 the plants result underused, and thus the number of plants chosen is too high. A reduction of the number of plants installed could lead to a more fruitful use of the plants. In Case 2, only one plant results underused (i.e., having capacity factor equal to 23%), whereas the other plants are quite well exploited.

Case 3 presents 12 plants having a capacity factor lying in the range 40%-50%, whereas the remaining plants have a capacity factor between 50% and 60%.

Finally, Case 4 presents three plants with capacity factor lower than 40% (i.e., from 28% to 37%), whereas all the other plants are well exploited (minimum about 51%).

From the results it is evident that the number of plants installed has a great impact and need to be carefully considered. The analysis carried out, in any case, neglects the presence of suitable gas network points: in the reality, the presence of real infrastructures will limit the potential nodes where PtG can be installed to a smaller number than the one considered here.

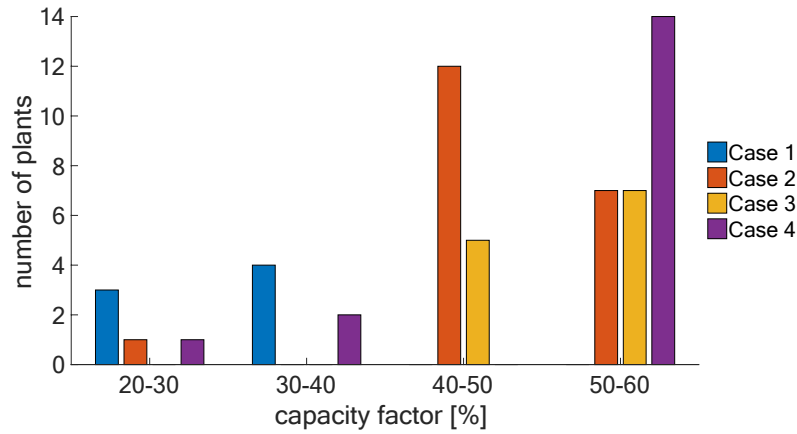


Figure 9. Capacity factors for the different cases of semi-urban network

In the case of the rural network, the results are summarized in Table 7. With respect the previous case, the minimum capacity factor results higher than 60% in all the cases, and reaches almost 90% in one case. The results in the table indicate also for this case that PtG can handle very well the issues created from PV generation installed at the end of relatively long lines, by maintaining a sufficiently high capacity factor.

Table 7. Annual capacity factors for the rural network

Case	PV penetration	Min capacity load [%]	Max capacity load [%]
5	40%	47.55 ⁴	-
6	80%	43.47	54.96
7	40%	47.10 ⁴	-
8	80%	48.50	56.0
9	40%	43.07	49.26
10	80%	45.68	50.88

A good performance index of the network is the value of the power losses, which are summarized in Table 8.

The value of the losses (in MWh and in percentage) is reduced in all the cases. This reduction is obtained thanks to the installation of the plants that help to improve the network operation.

Table 8. Network losses for both the semi-urban network and the rural network

Case	Power Losses [MWh]		Power Losses [%]		Case	Power Losses [MWh]		Power Losses [%]	
	pre	post	pre	post		pre	post	pre	post
1	2122.5	2314.9	0.95	0.20	5	1,149.8	1,128.9	2.22	1.82
2	3445.1	2902.4	7.36	0.69	6	2040.0	1,363.1	9.34	2.38
3	3779.0	3278.7	1.71	0.28	7	1142.5	1042.1	2.21	1.74
4	6517.5	4082.1	4.86	0.50	8	2,683.5	1,972.0	12.29	3.82

⁴ These cases require only one PtG plant.

9	1263.9	1,205.9	2.42	1.77
10	20,991	1358.0	7.68	2.51

420

421 Another performance indicator is the voltage magnitude (maximum and minimum), whose values for both semi-urban and
 422 rural networks are shown in Table 9. It is evident the effect of PtG to reduce the voltage at levels that are lying within the
 423 admissible ranges.

424 *Table 9 Minimum and Maximum voltage magnitude for both semi-urban and rural networks*

Case	Minimum voltage [pu]		Maximum voltage [pu]		Case	Minimum voltage [pu]		Maximum voltage [pu]	
	pre	post	pre	post		pre	post	pre	post
1	1.00	1.00	1.04	1.03	5	0.93	0.93	1.05	1.04
2	1.00	1.00	1.06	1.05	6	0.93	0.93	1.11	1.06
3	1.00	1.00	1.11	1.09	7	0.93	0.93	1.07	1.03
4	1.00	0.93	1.15	1.04	8	0.93	0.93	1.14	1.09
					9	0.93	0.92	1.05	1.01
					10	0.93	0.93	1.06	1.05

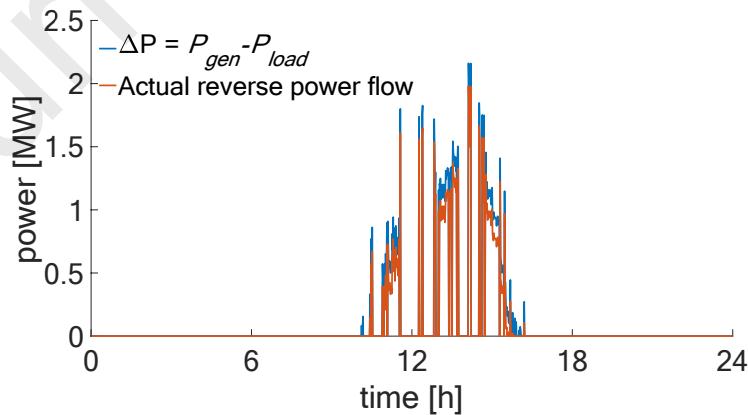
425

426 4.2 Network effect

427 This section aims to highlight the role of the network infrastructure in the proper evaluation of the effect of the PtG
 428 deployment.

429 In fact, some approaches existing in literature (e.g., [7]) do not consider the existence of the electrical infrastructure, but only
 430 the potential unbalance between local generation and loads. However, this approach could not be proper for solving completely
 431 the issue caused by the excess of RES.

432 Taking as example a particular day of Case 5⁵, the difference between generation and loads, without taking into account the
 433 network, is shown in Figure 10. The same figure also reports the actual reverse power flow existing in the network. The two
 434 curves are quite similar, but the first one overestimates the actual reverse power flow value.



435

436 *Figure 10. Comparison between the actual reverse power flow (with and without the network)*

437 For the sake of clarity, the rural network schematic is shown in Figure 11.

⁵ The day considered has as PV profile the one shown in Figure 5b, Month July.

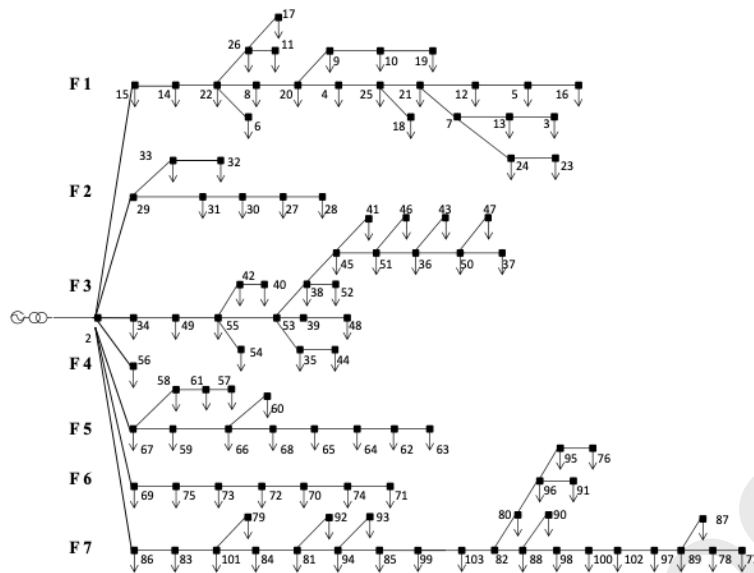


Figure 11. Rural network.

The installation of plants characterised by different size at node 2 (connected to the network slack node) instead of node 83 (as in Case 5) leads to the results shown in Table 10. The solutions show that the reverse power flow issue can be almost completely solved by using a plant with smaller size than the one referring at Case 5. This may lead to think that the solution of Case 5 could be not be optimal, because of the size. However, the capacity factor highlights that the installation of the plant at the node connected to the slack bus does not guarantee a good utilisation of the potential of the plant and thus the installation node should be carefully chosen. Furthermore, the use of the plant with the position and size of Case 5 allows improving the network conditions, in terms of power losses and reverse power flow. This simple example aims to be an effective way to show the importance of the network information to capture all the aspects regarding the new operation of the electrical system when new devices are installed.

Table 10. Comparison between the network performance without PtG, with PtG installed without optimisation process and with optimisation process (referring to a day of Case 5)

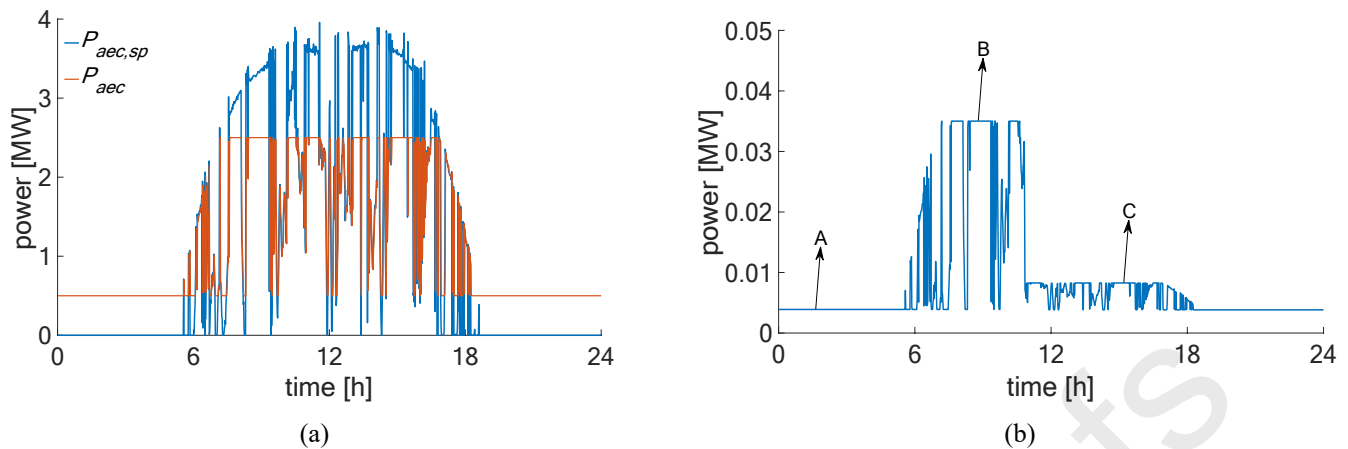
Size [MW]	Reverse power flow [MWh]	Reverse power flow [min]	Power Losses [MWh]	Power Losses [%]	Capacity factor [%]
0 (no PtG)	2.16	151	3.08	2.29	-
0.5	1.026	143	3.09	2.24	50.81
1	0.284	139	3.096	2.20	44.21
1.5	0.062	135	3.102	2.17	36.02
2	0.025	120	3.108	2.14	30.44
2.5	0.022	110	3.114	2.11	27.03
2.5	0	0	3.00	1.85	69.22

4.3 Response of the PtG model

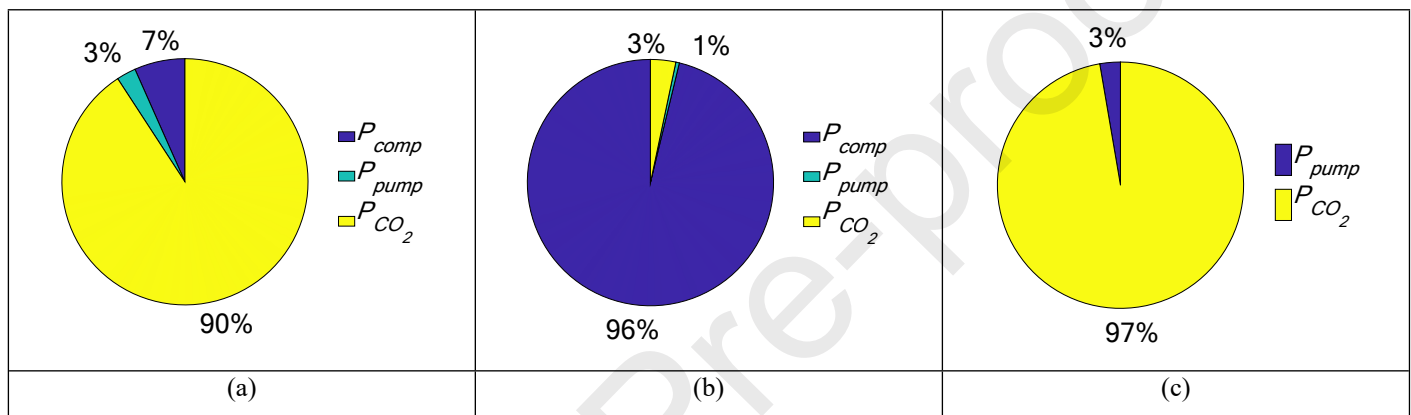
The PtG model provides in output the following quantities:

- 455 • Power profile sent by the control system to the electrolyser $P_{elec,sp}$
- 456 • Power profile of the electrolyser P_{elec}
- 457 • Power profile of the auxiliary services P_{aux} , referring to i) the CO₂ compression system, ii) the circulation of H₂O, iii) the
458 compression of the H₂, and iv) the water heating.
- 459 • The hydrogen flow rate sent to the tank $\varphi_{H_2,tank}$ [kmol/s]
- 460 • The hydrogen sent to the methanation unit directly from the electrolyser $\varphi_{H_2,dir}$ [kmol/s]
- 461 • The hydrogen sent to the methanation unit from the tank after compression $\varphi_{H_2,tank,meth}$ [kmol/s]
- 462 • The level of the hydrogen tank [%]
- 463 • The SNG produced seen as power profile [MW] or energy profile [MWh]

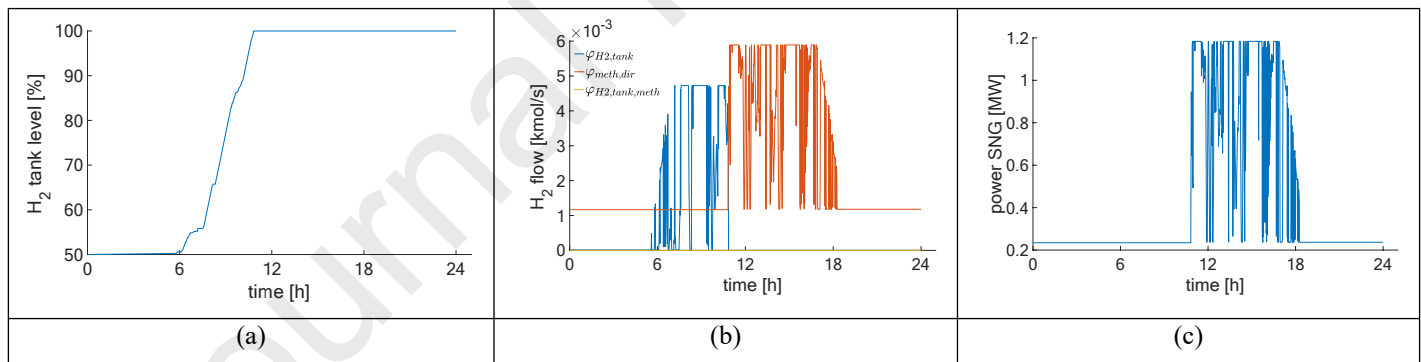
464 With reference to the same day considered in Section 4.2 of Case 5, $P_{elec,sp}$, P_{elec} and P_{aux} , are shown in Figure 12. In Figure
465 12(a), it is evident the saturation imposed by the nominal power of the plant. Furthermore, the minimum power required by the
466 AEC is different from zero and has to be provided by the main network. Figure 12(b), instead, shows the power related to the
467 auxiliary services. Three zones with different auxiliary service power exist, and each of them is characterized by different
468 contributions, as highlighted in Figure 13. More specifically, during the night no excess of electrical power is available for the
469 PtG plant; therefore, it operates at the minimum power load corresponding to 20 % of the nominal installed power. As illustrated
470 in Figure 13(a) auxiliary consumptions are principally due to the CO₂ compression, while water pumping and H₂ compression
471 are marginal contributions. Subsequently, in the first part of the day (between 6 h and 11 h) the electrical availability increases,
472 and the electrolyser could work in its whole operative range (from 20% to 100%); thus, it produces a large amount of H₂, which
473 is mainly stored in the tank until it is completely full. Hence, H₂ compression represents 96% of all auxiliary consumptions, as
474 shown in Figure 13(b). At the same time, the methanation unit operates at the minimum power load for allowing the tank to be
475 filled, in fact, the CO₂ compression represents 3% of the auxiliary consumptions even though it is the minimum power
476 consumption for compressing CO₂. Lastly, in the second part of the day (between 11 h and 18 h), both the electrolyser and the
477 methanation unit work in their whole operational range and the H₂ tank is entirely full. More in detail, as depicted in Figure
478 13(c), H₂ has not to be compressed and the CO₂ compression cost increases as the CO₂ flow rises (H₂ and CO₂ are fed in
479 stoichiometric ratio to the methanation unit). Furthermore, all these aspects of the process are clearly illustrated in Figure 14. As
480 shown in Figure 14 (a and b), the H₂ tank is filled during the first hours of the day, when there is a large excess of electrical
481 energy availability. Subsequently, both the electrolyser and the methanation unit operate for producing SNG, as depicted in
482 Figure 14 (b and c). In this case study (Case 5), the alkaline electrolyser absorbs 28 MWh of electricity, which is converted into
483 237.4 kmol of H₂ (15.8 MWh, LHV basis). Initially, the produced H₂ is partially stored in the tank (50.9 kmol) until it is
484 completely full; subsequently, the H₂ flow is sent to the methanation unit for producing SNG (10.4 MWh, LHV basis). In this
485 case study, the auxiliaries require 0.21 MWh of electrical energy during the whole day. It is worth noting that the tank is not
486 discharged, because the minimum operative power set for the electrolyser was assumed to be 20% (as specified in Section 2),
487 which is equal to the minimum flow required by the methanation unit. However, the model includes also the storage system,
488 which can intervene if a different control is applied.



489 Figure 12. Electrical quantities provided by the PtG model: (a) input power profiles and (b) power profile of the auxiliary services.



490 Figure 13. Composition of the auxiliary services in the different periods of the day.



491 Figure 14. (a) H_2 tank filling, (b) H_2 molar flow rates and (c) SNG productivity of the PtG plant.

492 5. Conclusions

493 This paper has presented a detailed study regarding the impact of PtG technology on the electrical distribution system. The
 494 study takes into account both electrical aspects and information related to the process chain leading to the SNG production.

495 Thanks to the physical model of the PtG plant, the evaluation of the values of its internal variables (e.g., hydrogen flows) can
 496 be checked, and this allows acting on the downstream portion of the plant, i.e., methanation plant and hydrogen buffer.

497 Furthermore, the request of energy to supply the auxiliary services can be successfully evaluated. It is worth noting that the
 498 plant layout can be changed, both in terms of control and in terms of components adopted.

499 From the electrical point of view, this paper shows that the evaluation of the impact of PtG plants on the distribution system

500 has to consider the *local* network conditions, because different network samples lead to different problem to be solved. The
501 knowledge of the type of network where the plants will be installed is thus fundamental, and has been presented here by
502 considering two network samples.

503 Furthermore, the level of RES penetration is another important aspect to be taken into account, due to the different network
504 issues introduced. From the paper results it was evident the difference between alert and emergency network operation, which
505 linked to different variables (reverse power flow and network constraints, respectively).

506 For the semi-urban network, the number and the sizes of the PtG plants are higher than the ones used for the rural network,
507 due to the higher number of nodes and higher load. The results obtained are significantly good, with a reduction of the reverse
508 power flow energy falling in the range 78-100%, with better performances for lower PV penetration. Furthermore, in all the
509 cases the installation of PtG plants has reduced the network losses of the network and no undervoltage problems have been found
510 during the year, even with scarce solar radiation (i.e., in winter months).

511 By considering the rural network, the case $0 < L \leq 0.9$ km sees a reduction of the reverse power flow energy falling in the range
512 92-100%, whereas in the case $2 \leq L \leq 3$ km the reduction lies in the range 83-100%. In all cases, the installation of PtG is also
513 able to alleviate the problems due to violations of constraints if PtG is absent, by reaching the complete elimination of these
514 violations for the lower PV penetrations.

515 The load factor of the plants provides information on how much a PtG plant is used: these values strongly depend on the
516 network conditions (correlated to the PV penetration value), as well as on the positioning of the PtG and on the size. The values
517 of capacity factors are higher for the rural network than for the semi-urban network: in fact, the minimum capacity factor values
518 for the rural network fall around 50%, whereas for the rural network the minimum capacity factors fall down to 21%. This
519 suggests that the installation of PtG plants at the level of distribution system has to be made by considering the local
520 characteristics of the network.

521 All the performances of the plants have been obtained by considering the *network effect*, and has been shown with an effective
522 evidence that neglecting its presence can lead to wrong results (e.g., lower capacity factor or slight over-estimation of the reverse
523 power flow).

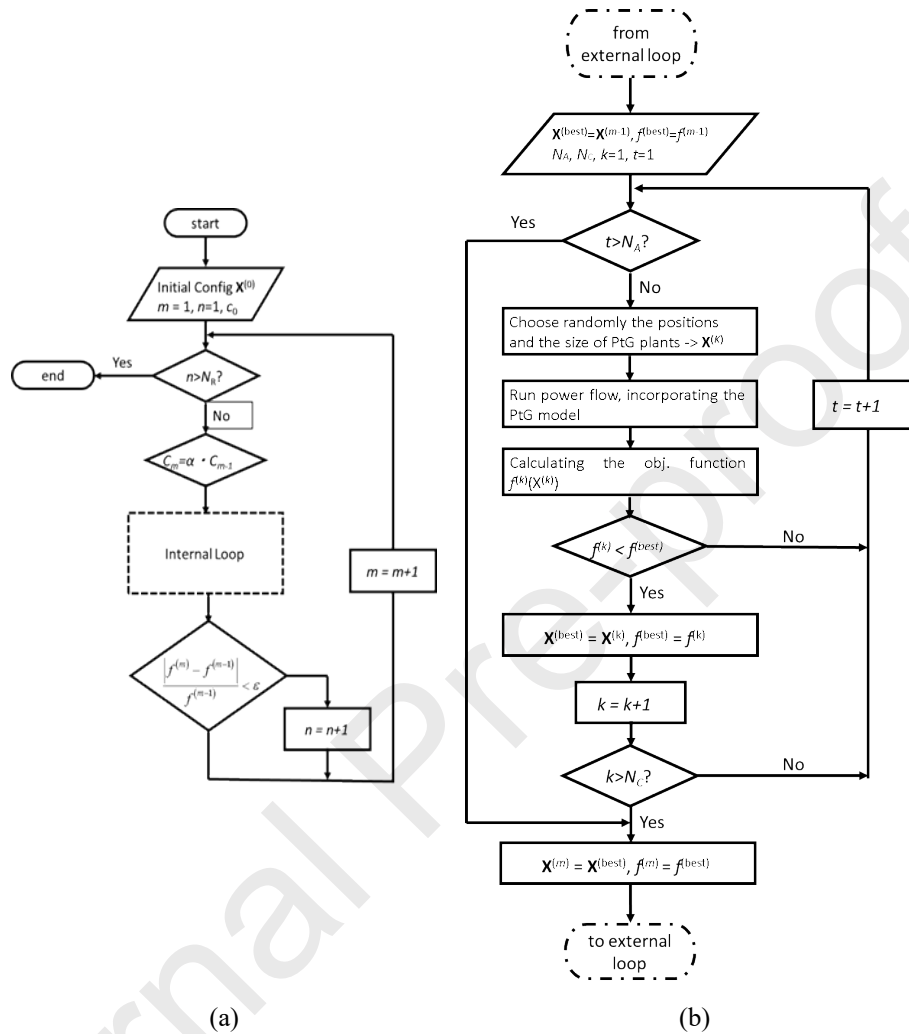
524 In conclusion, it can be said that the addition of PtG systems in a distribution network can stabilise the network even for very
525 high (even extreme) renewable energy penetrations, thus increasing the ability of a network to host higher penetration of
526 intermittent generation. The deployment of the plants in the real network needs to be considered the presence of a proper gas
527 network, to be fed with the renewable synthetic gas that, having the same characteristics of the natural gas, opens new
528 perspectives to decarbonise the entire energy system.

529

530 **Appendix**

531 The Simulated Annealing (SA) algorithm is composed of an external loop (shown in Figure 15a) and an internal loop (shown
532 in Figure 15b).

533



534 *Figure 15. The external loop (a) and the internal loop (b) of the SA used for siting and sizing.*

535 The external cycle depends on a control parameter called C , whose initial value is named C_0 . For every iteration $m > 0$ of the
536 external cycle, the control parameter is updated with a certain velocity described by the cooling rate, i.e.:

537

$$C_m = \alpha \cdot C_{m-1} \quad (12)$$

538 The stop criterion of the external cycle is based on the persistence of the solution found so far: once the solution found persists
539 (or the changes are below a certain threshold) for at least N_R successive iterations, the external cycle stops⁶

540 At each iteration of the external cycle, the internal cycle is run. For every iteration m of the external cycle, the inputs of the
541 internal cycle are:

⁶ This kind of stop criterion is typical of many heuristics existing in the literature and avoids fixing a priori the limit number of iterations, but only the number of iterations in which the same solution persists.

- 542 • *Initial configuration* $\mathbf{X}^{(best)}$ and its objective function $f^{(best)}$: it refers to the best configuration found so far (the solution
- 543 provided as output at the iteration $m-1$)
- 544 • *Value of the control parameter* C_m
- 545 • *Number of solutions to be analysed* N_A
- 546 • *Number of solutions to be accepted* N_C

547 The last two inputs are necessary for the stopping criterion of the internal cycle, which is structured as follows: the internal
548 cycle stops when either N_C or N_A are reached. The first condition is usually reached with high C_m (i.e., when many new solutions
549 are accepted), whereas the second condition is usually reached with low C_m (i.e., when the number of accepted solutions
550 decreases, up to the final internal cycles before stopping, in which there is no acceptance of new solutions). In addition, the seed
551 for random number extractions is fixed before starting the iterative process, to enable repeatability of the results obtained.

552 Acknowledgment

553 This contribution has received funding from the European Union's Horizon 2020 research and innovation programme under
554 grant agreement No. 691797 (project STORE&GO). The paper only reflects the authors' views and the European Union is not
555 liable for any use that may be made of the information contained herein.

556 The Authors would like to thank Mr. Luca Serra, for having provided his support in the calculation part.

557 References

- 558 [1] A. Mazza, M. Cavana, E. L. Mercado Medina, G. Chicco, and P. Leone, "Creation of Representative Gas Distribution
559 Networks for Multi-vector Energy System Studies," *Proc. IEEE International Conference on Environment and
560 Electrical Engineering and 2019 IEEE Industrial and Commercial Power Systems Europe (EEEIC / I&CPS Europe)*, 11-
561 14 June 2019.
- 562 [2] Z. Yang, C. Gao, and M. Zhao, "Coordination of integrated natural gas and electrical systems in day-ahead scheduling
563 considering a novel flexible energy-use mechanism," *Energy Convers. Manag.*, vol. 196, pp. 117–126, 2019.
- 564 [3] A. Mazza, E. Bompard, and G. Chicco, "Applications of power to gas technologies in emerging electrical systems,"
565 *Renew. Sustain. Energy Rev.*, vol. 92, pp. 794–806, Sep. 2018.
- 566 [4] S. Schiebahn, T. Grube, M. Robinius, L. Zhao, A. Otto, B. Kumar, M. Weber and D. Stolten, "Power to Gas," Chapter
567 39 in *Transition to Renewable Energy Systems*, D. Stolten and V. Scherer (Eds.), Wiley, 2013, pp. 813–848.
- 568 [5] K. Ghaib and F.-Z. Z. Ben-Fares, "Power-to-Methane: A state-of-the-art review," *Renew. Sustain. Energy Rev.*, vol. 81,
569 pp. 433–446, Jan. 2018.
- 570 [6] M. Robinius *et al.*, "Power-to-Gas: Electrolyzers as an alternative to network expansion – An example from a
571 distribution system operator," *Appl. Energy*, vol. 210, pp. 182–197, Jan. 2018.
- 572 [7] F. Salomone, E. Giglio, D. Ferrero, M. Santarelli, R. Pirone, and S. Bensaid, "Techno-economic modelling of a Power-
573 to-Gas system based on SOEC electrolysis and CO₂ methanation in a RES-based electric grid," *Chem. Eng. J.*, vol. 377,
574 art. 120233, Dec. 2019.

- 575 [8] T. Estermann, M. Newborough, and M. Sterner, "Power-to-gas systems for absorbing excess solar power in electricity
576 distribution networks," *Int. J. Hydrogen Energy*, vol. 41, no. 32, pp. 13950–13959, Aug. 2016.
- 577 [9] C. Park, F. Bigler, and P. Korba, "Power-to-Gas Concept for Integration of Increased Photovoltaic Generation into the
578 Distribution," *Energy Procedia*, vol. 99, pp. 411–417, Nov. 2016.
- 579 [10] B. Simonis and M. Newborough, "Sizing and operating power-to-gas systems to absorb excess renewable electricity,"
580 *Int. J. Hydrogen Energy*, vol. 42, no. 34, pp. 21635–21647, Aug. 2017.
- 581 [11] N. A. El-Taweel, H. Khani, and H. E. Z. Farag, "Voltage regulation in active power distribution systems integrated with
582 natural gas grids using distributed electric and gas energy resources," *Int. J. Electr. Power Energy Syst.*, vol. 106, pp.
583 561–571, Mar. 2019.
- 584 [12] A. R. Dalmau, D. M. Perez, I. Diaz de Cerio Mendaza, and J. R. Pillai, "Decentralized voltage control coordination of
585 on-load tap changer transformers, distributed generation units and flexible loads," *Proc. IEEE Innovative Smart Grid
586 Technologies - Asia (ISGT ASIA)*, 3-6 Nov. 2015.
- 587 [13] I. D. de Cerio Mendaza, B. Bak-Jensen, and Z. Chen, "Alkaline electrolyzer and V2G system DIGSILENT models for
588 demand response analysis in future distribution networks," *Proc. IEEE Grenoble Conference*, 16-20 June 2013.
- 589 [14] I. Diaz de Cerio Mendaza, B. P. Bhattarai, K. Kouzelis, J. R. Pillai, B. Bak-Jensen, and A. Jensen, "Optimal sizing and
590 placement of power-to-gas systems in future active distribution networks," *Proc. IEEE Innovative Smart Grid
591 Technologies - Asia (ISGT ASIA)*, 3-6 Nov. 2015.
- 592 [15] H. Khani, N. El-Taweel, and H. E. Z. Farag, "Real-time optimal management of reverse power flow in integrated power
593 and gas distribution grids under large renewable power penetration," *IET Gener. Transm. Distrib.*, vol. 12, no. 10, pp.
594 2325–2331, 2018.
- 595 [16] H. Khani, N. El-Taweel, and H. E. Z. Farag, "Power Congestion Management in Integrated Electricity and Gas
596 Distribution Grids," *IEEE Syst. J.*, vol. 13, no. 2, pp. 1883–1894, 2019.
- 597 [17] H. Khani, N. El-Taweel, and H. E. Z. Farag, "Power Loss Alleviation in Integrated Power and Natural Gas Distribution
598 Grids," *IEEE Trans. Ind. Informatics*, vol. 15, no. 12, pp. 6220–6230, 2019.
- 599 [18] European Project STORE&GO, web: <https://www.storeandgo.info/>
- 600 [19] E. Giglio, A. Lanzini, M. Santarelli, and P. Leone, "Synthetic natural gas via integrated high-temperature electrolysis and
601 methanation: Part I—Energy performance," *J. Energy Storage*, vol. 1, pp. 22–37, Jun. 2015.
- 602 [20] M. Samavati, M. Santarelli, A. Martin, and V. Nemanova, "Thermodynamic and economy analysis of solid oxide
603 electrolyser system for syngas production," *Energy*, vol. 122, pp. 37–49, 2017.
- 604 [21] M. Bailera, P. Lisbona, L. M. Romeo, and S. Espatolero, "Power to Gas projects review: Lab, pilot and demo plants for
605 storing renewable energy and CO₂," *Renew. Sustain. Energy Rev.*, vol. 69, pp. 292–312, Mar. 2017.

- 606 [22] E. Giglio, A. Lanzini, M. Santarelli, and P. Leone, "Synthetic natural gas via integrated high-temperature electrolysis and
607 methanation: Part II—Economic analysis," *J. Energy Storage*, vol. 2, pp. 64–79, 2015.
- 608 [23] M. Götz *et al.*, "Renewable Power-to-Gas: A technological and economic review," *Renew. Energy*, vol. 85, pp. 1371–
609 1390, Jan. 2016.
- 610 [24] S. McDonagh, R. O'Shea, D. M. Wall, J. P. Deane, and J. D. Murphy, "Modelling of a power-to-gas system to predict
611 the levelised cost of energy of an advanced renewable gaseous transport fuel," *Appl. Energy*, vol. 215, pp. 444–456,
612 2018.
- 613 [25] E. Giglio *et al.*, "Power-to-Gas through High Temperature Electrolysis and Carbon Dioxide Methanation: Reactor
614 Design and Process Modeling," *Ind. Eng. Chem. Res.*, vol. 57, no. 11, pp. 4007–4018, 2018.
- 615 [26] O. Schmidt, A. Gambhir, I. Staffell, A. Hawkes, J. Nelson, and S. Few, "Future cost and performance of water
616 electrolysis: An expert elicitation study," *Int. J. Hydrogen Energy*, vol. 42, no. 52, pp. 30470–30492, 2017.
- 617 [27] Ø. Ulleberg, T. Nakken, and A. Eté, "The wind/hydrogen demonstration system at Utsira in Norway: Evaluation of
618 system performance using operational data and updated hydrogen energy system modeling tools," *Int. J. Hydrogen
619 Energy*, vol. 35, no. 5, pp. 1841–1852, Mar. 2010.
- 620 [28] E. A. Morosanu, F. Salomone, R. Pirone, and S. Bensaid, "Insights on a Methanation Catalyst Aging Process: Aging
621 Characterization and Kinetic Study," *Catalysts*, vol. 10, no. 3, art. 283, Mar. 2020.
- 622 [29] P. Marocco *et al.*, "CO₂ methanation over Ni/Al hydrotalcite-derived catalyst: Experimental characterization and kinetic
623 study," *Fuel*, vol. 225, pp. 230–242, Aug. 2018.
- 624 [30] E. A. Morosanu, A. Saldivia, M. Antonini, and S. Bensaid, "Process Modeling of an Innovative Power to LNG
625 Demonstration Plant," *Energy & Fuels*, vol. 32, no. 8, pp. 8868–8879, Aug. 2018.
- 626 [31] R. K. Sinnott, *Coulson & Richardson's Chemical Engineering Design*, 4th ed., vol. 6. Oxford, 2005.
- 627 [32] D. E. Seborg, T. F. Edgar, and D. A. Mellichamp, *Process Dynamics and Control*, 2nd editio. John Wiley & Sons, 2003.
- 628 [33] B. A. Ogunnaike and W. H. Ray, *Process Dynamics, Modeling and Control*. Oxford University Press, 1994.
- 629 [34] R. H. Perry, D. W. Green, and J. O. Maloney, *Perry's Chemical Engineers' Handbook 7th edition*, 7th ed. The McGraw-
630 Hill Companies, 1999.
- 631 [35] K. R. Sundaresan and P. R. Krishnaswamy, "Estimation of Time Delay Time Constant Parameters in Time, Frequency,
632 and Laplace Domains," *Can. J. Chem. Eng.*, vol. 56, no. 2, pp. 257–262, 1978.
- 633 [36] N. Jenkins, J. B. Ekanayake, and G. Strbac, *Distributed Generation*. London: IER Renewable Energy Series, 2010.
- 634 [37] Enel-Energia, "Enel Energia a tutto storage," <https://corporate.enel.it/it/media/news/d/2015/12/enel-energia-a-tutto->

- 635 *storage* (in Italian).
- 636 [38] L. H. Fink and K. Carlsen, "Operating Under Stress and Strain.," *IEEE Spectr.*, vol. 15, no. 3, pp. 48–53, 1978.
- 637 [39] A. Mazza, E. Carpaneto, G. Chicco, and A. Ciocia, "Creation of Network Case Studies with High Penetration of
638 Distributed Energy Resources," *Proc. 53rd International Universities Power Engineering Conference (UPEC 2018)*, 4-7
639 Sept. 2018.
- 640 [40] E. Carpaneto, G. Chicco, and J. Sumaili Akilimali, "Characterization of the loss allocation techniques for radial systems
641 with distributed generation," *Electr. Power Syst. Res.*, vol. 78, no. 8, pp. 1396–1406, Aug. 2008.
- 642 [41] A. Mazza and G. Chicco, "Losses Allocated to the Nodes of a Radial Distribution System with Distributed Energy
643 Resources — A Simple and Effective Indicator," *Proc. International Conference on Smart Energy Systems and
644 Technologies (SEST)*, 9-11 Sept. 2019.
- 645 [42] G. Pretticco, M.G. Flammini, N. Andreadou, S. Vitiello, G. Fulli, and M. Masera, "Distribution System Operators
646 observatory 2018-Overview of the electricity distribution system in Europe", EUR 29615 EN, Publications Office of the
647 European Union, Luxembourg, 2019.
- 648 [43] E. Bompard, G. Chicco, A. Mazza, and S. Bensaid, "Deliverable 6.4 Report on the model of the power system with
649 PtG," European Project STORE&GO, 2019.
- 650 [44] A. Bracale *et al.*, "Analysis of the Italian distribution system evolution through reference networks," *Proc. 3rd IEEE PES
651 Innovative Smart Grid Technologies Conference Europe*, 14-17 Oct. 2012.
- 652 [45] J.M. Bright, *Bright Solar Resource Model*, web: <https://jamiembright.github.io/BrightSolarModel/>
- 653 [46] D. Shirmoharmnadi, H. W. Hong, A. Semlyen, and G. X. Luo, "A compensation-based power flow method for weakly
654 meshed distribution and transmission networks," *IEEE Trans. Power Syst.*, vol. 3, no. 2, pp. 753–762, 1988.
- 655 [47] P. J. M. van Laarhoven and E. H. L. Aarts, *Simulated Annealing: Theory and Applications*. Dordrecht, Holland: D.Reidel
656 Publ. Company, 1987.